ACS APPLIED MATERIALS & INTERFACES

Research Article

www.acsami.org

Interfacial Structure and Photocatalytic Activity of Magnetron Sputtered TiO_2 on Conducting Metal Substrates

Svava Davíðsdóttir,*[,†] Jean-Pierre Petit,[‡] Michel Mermoux,[§] Rajashekhara Shabadi,[⊥] Stela Canulescu,[#] Klaus P. Almtoft,[∥] Kai Dirscherl,[△] and Rajan Ambat[†]

[†]Division of Materials and Surface and Engineering, Department of Mechanical Engineering, Technical University of Denmark, DK-2800 Kongens Lyngby, Denmark

[‡]SIMAP and [§]LEPMI, Université Grenoble Alpes/CNRS, F-38000 Grenoble, France

[⊥]Unité Matériaux et Transformations, C6, Université Lille, 59655 Villeneuve 'Ascq, France

[#]Department of Photonics Engineering, Technical University of Denmark, DK-4000 Roskilde, Denmark

[∥]Tribology Centre, Danish Technological Institute, Teknologiparken, Building 18, Kongsvang Allé 29, DK-8000 Aarhus C, Denmark

[△]Danish Fundamental Metrology, Matematiktorvet 307, DK-2800 Kongens Lyngby, Denmark

ABSTRACT: The photocatalytic behavior of magnetron sputtered anatase TiO_2 coatings on copper, nickel, and gold was investigated with the aim of understanding the effect of the metallic substrate and coating-substrate interface structure. Stoichiometry and nanoscale structure of the coating were investigated using X-ray diffraction, Raman spectroscopy, atomic force microscope, and scanning and transmission electron microscopy. Photocatalytic behavior of the coating was explored by using optical spectrophotometry and electrochemical methods via photovoltage, photocurrent, and scanning kelvin probe microscopy measurements. The nature of the metal substrate and coating-substrate interface had profound influence on the photocatalytic behavior. Less photon energy was required for TiO_2 excitation on a nickel substrate, whereas TiO_2 coating on copper showed a higher band gap attributed to quantum confinement. However, the TiO_2 coating on gold exhibited behavior typical of facile transfer of electrons to and from the CB, therefore requiring only a small amount of photon energy to make the TiO_2 coating conductive.

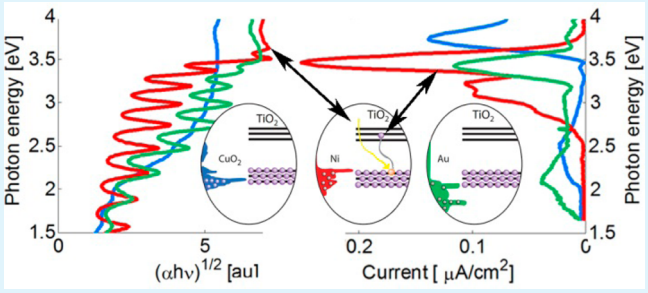

KEYWORDS: *photocatalytic, anatase, metallic substrate, photoelectrochemistry, photoabsorption, Raman spectroscopy*

INTRODUCTION

Innovative applications of the photocatalytic titanium dioxide (TiO_2) material have increased in the past several years. The photocatalytic abilities of anatase have been exploited in air and water purification using its heterogeneous photocatalytic oxidation (PCO)[1] and advanced oxidation process (AOP)[2] capabilities, respectively. The TiO_2 coating produced by a chemical vapor deposition process on a glass substrate is used widely as self-cleaning glass.[3] Most of the studies on TiO_2 have focused on the material in powder form or as a thin coating on a glass substrate.[4] New applications for TiO_2 are continuously being explored, and recently, the use of TiO_2 as a coating on conducting metal substrates, such as aluminum and steel[5,6] and for biomedical applications involving bioimplants was investigated. For biocompatible implants, the photocatalytic activity of the surface was used in sterilization of the implant and to increase tissue formation resulting from the remnant activity once the coated implant was introduced into the body.[7−9] The anatase TiO_2 coatings have also been studied for applications involving resistance random access memories (RRAMs).[10]

An important aspect of the photocatalytic activity of anatase TiO_2 is its self-cleaning ability, which can be exploited for a number of structural applications. Of major interest is the TiO_2 coating in contact with metal or metal alloy substrates. It has been reported that the photocatalytic behavior of TiO_2 on a conducting substrate is different from that on a nonconducting substrate due to the possibility of electron transfer, which is also a function of the interface structure.[6,5,11]

Various metal atoms are used as doping agent with TiO_2 to increase its photocatalytic activity by decreasing the band gap, which is based on the concept of extracting electrons to reduce the electron−hole recombination. For example, doping by gold (Au) and copper (Cu) is known to improve the photocatalytic activity of TiO_2.[11−13] Several explanations have been given for the improvement of photocatalytic activity of Cu-doped TiO_2 coating. In particular, Paola et al. found that Cu can be reduced into its metallic state, Cu^0, and therefore can act as a cocatalyst.[12]

The use of Au as a doping element or as incorporated particles with TiO_2 has been reported to increase the rate of

Received: September 1, 2014
Accepted: December 1, 2014
Published: December 1, 2014

charge separation as the electrons are adsorbed into the metal, thereby increasing the photocatalytic activity.[11,14] However, it has also been reported that Au-doping in TiO_2 decreases the photocatalytic activity due to the lack of ability of the coating to form OH radicals, which are used for the photocatalytic reaction.[14]

Utilizing nickel as a doping element in TiO_2 has not been studied extensively. The position of the energy band (the overlapping valence and conduction band) for Ni is slightly above the valence band (VB) of titanium dioxide. Therefore, Ni interacts strongly with the anatase through the formation of Ni−O−Ti bonds, with the Ni 3d orbital interacting strongly with the VB of TiO_2. The maximum energy of the VB of TiO_2 is raised significantly and, simultaneously, a new vacant orbital level is formed close to the conduction band (CB) of TiO_2. At the interface between the TiO_2-coating and the Ni-substrate less photon energy is needed for electron excitation, and the electrons from Ni are excited to the CB of TiO_2. The holes can be used for oxidation, whereas the electrons are consumed by the reduction reactions. The holes created in the raised VB will have weaker oxidation power than the holes that migrated or formed in the VB of the unmodified TiO_2.[15] A single study[11] reported improved photocatalytic activity compared to glass substrate when Au and Cu where used as a substrate for TiO_2 coatings. Moreover, the use of gold was reported to reduce the band gap of TiO_2.

When the TiO_2 coating is in contact with a metal or semiconductor with a lower band gap than that of TiO_2, the orbitals from the substrate and TiO_2 can merge to form new orbitals. Because of this interaction, the newly formed orbitals can have different energy states, with energy between the bands of the TiO_2. The sub-band gap states in TiO_2 have been reported in the literature.[16−18] When the band energy level of the substrate coating interfaces is spaced between the band gap of TiO_2, it can influence the photocatalytic behavior by reducing the energy of light needed for photocatalytic activation. The band structure and conductivity of metals and the location of the energy state can influence the electron transfer, either by facilitating the electron transition or by working as recombination centers depending on the energy position of the bands.[19]

The VB and CB bands are overlapping in metals allowing the electrons to move freely and act as conductors. The potential of the metal (Fermi level) is determined by the respective locations of the VB and CB. If the potential of the metal lies close to the CB minimum of TiO_2, an electron from the metal may be transferred to the CB giving the TiO_2 coating more conductivity. When the potential of the metal lies in between the bands of titanium dioxide, the metal energy band may be used for transferring electrons from the VB to CB during excitation, thereby, reducing the energy of light needed for activation. It is also important to note that Schottky barrier will be present in all the cases due to high work function of the substrate materials (4.8, 4.25, and 4.25 eV respectively for Au, Ni, Cu).

The present study focuses on investigating the behavior of magnetron sputtered anatase TiO_2 coatings on three substrate materials, Ni, Cu, and Au, with the aim of understanding the effect of substrate and substrate-coating interface on the photocatalytic activity. Our previous investigations showed that the conducting substrates and interfaces significantly influence the photocatalytic behavior of TiO_2.[5,20] The selected metals for this study have higher Gibbs free energy for oxide formation than the TiO_2. Several analytical methods are employed to provide insight into the interaction between the TiO_2 coating and substrate, and its effect on photocatalysis. This includes detailed nonstructural investigations using scanning electron microscopy (SEM) and transmission electron microscopy (TEM), atomic force microscope (AFM), Raman spectroscopy, and a combination of electrochemical methods such as electrochemical impedance spectroscopy (EIS), scanning kelvin probe force microscopy, and optical methods such as spectrophotometry and light frequency dependent photocurrent measurements.

EXPERIMENTAL SECTION

Substrate Material. Substrates used for the coating were pure Cu, electroplated Ni on Cu substrate, and electroplated Au on Cu substrate with thin nickel layer. The Ni plating was done using a commercial solution of Superbright Nickel SLOTONIK 40, whereas Au was plated using a commercial solution ECF64. All the substrates were cleaned prior deposition.

Preparation of the TiO_2 Coatings. The TiO_2 coatings were deposited by pulsed DC magnetron sputtering using an industrial CemeCon CC800/9 SinOx coating unit. The sputtering chamber was equipped with four magnetrons, each mounted with a 500 mm × 88 mm Ti target (purity 99.5 wt %). A pulsed DC power of 2 kW was applied to each magnetron. The depositions were carried out in an argon/oxygen atmosphere at a total pressure of about 1050 mPa. The Ar/O_2 gas flow ratio was 400 sccm/180 sccm, resulting in stoichiometric TiO_2 coatings. The deposition temperature of approximately 150 °C was controlled by a resistive heater. The deposition rate was 2.4 nm/min. All the samples were deposited in the same batch ensuring identical deposition conditions.

Photoelectrochemical Testing. Electrochemical measurements were employed to provide information about the photon excitation voltage measured with open circuit potential (OCP), the charge-transfer characteristics of the TiO_2 coated sample done with electro impedance spectroscopy (EIS), and the photo current generation as a function of wavelength of the incident UV light (photoelectrochemical spectroscopy (PES)). The PES method allows the detection of the possible range of wavelengths at which the photo current maximum occurs in comparison with structure of the coating.

A standard three-electrode electrochemical cell set up was used for the measurements. The specimen was loaded on the other side of the cell facing the quartz window. The reference electrode used for the measurement was Hg/Hg_2SO_4/saturated K_2SO_4 in order to avoid any chloride contamination to the solution. The counter electrode was platinum. The electrolyte for all experiments was deionized water with analytical grade 0.1 M $NaNO_3$ for increasing the conductivity of the solution. The specimen was pressed against an O-ring exposing a TiO_2 surface.

The OCP and EIS mesurements were carried out by exposing TiO_2 surface area of 9.6 cm^2 to the solution. The volume of the electrolyte was 550 mL. The UV lamp was a Philips home solarium, and it was placed at distance of 35 cm from the sample. The potentiostat used for the OCP experiments was from Gill AC BI-STAT, and for the EIS measurements, a potentiostat from Bio Logic, VSP, was used. The impedance measurements were performed from 1 to 1000 Hz with potentials ranging from −0.4 V to +0.74 V.

The PES experiments were carried out with an exposed surface area of 25 mm^2. The measurements were recorded under modulated light conditions, using a lock−in technique. A PAR 273 A (EG&G Instruments) potentiostat equipped with the/92 impedance interface was used to control the electrochemical cell. A voltage proportional to the overall electrochemical current, issued from the latter interface, was applied to the signal input of a lock−in amplifier (Stanford Research SR830). The synchronization signal delivered by the light chopper (PAR 197, EG&G Instruments) was applied to the reference input of the lock−in amplifier, allowing the extraction of the modulated

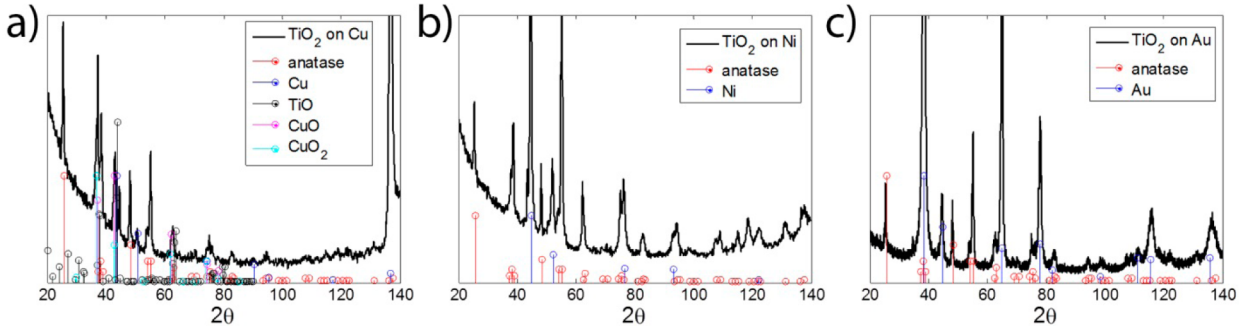

Figure 1. X-ray diffraction patterns obtained for TiO_2 coatings on various substrates: (a) Cu, (b) Ni, and (c) Au.

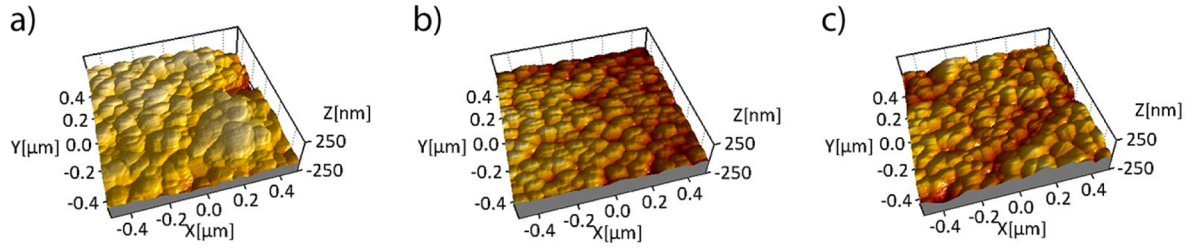

Figure 2. AFM pictures showing top surface of the TiO_2 coating on various substrates: (a) Cu, (b) Ni, and (c) Au.

photocurrent (modulus and phase shift) from the overall electrochemical current.

A 150 W xenon arc bulb (Newport, model 6255) interface with a triple grating monochromator (Newport, model 74125) was used as the light source, providing monochromatic photon fluxes at variable wavelengths with a typical spectral width of ±1 nm. It is expected that the photon fluxes delivered by the light source are different at each wavelength, and the optical path from the source to the sample does absorb photons differently when varying the wavelength.

The measured photocurrents (I_{PH}), were converted to values proportional to the quantum yield (J_{PH}). To obtain the J_{PH} values, a calibrated silicon photodiode (Newport, model 918D-UV-OD3R) was used to measure the photon fluxes at the sample position. The normalized photon flux at each wavelength $\Phi_N(h\nu)$ was calculated by dividing the actual photon flux $\Phi(h\nu)$ by its maximum value. The J_{PH} values were calculated using eq 1.

$$J_{PH} = \frac{I_{PH}}{\Phi_N(h\nu)} \quad (1)$$

The spectra were measured at five different applied potentials for each sample to a examine possible changes in the photocurrent upon varying the band bending in TiO_2. The sample was polarized at the selected potential, while illuminated at the lowest photon energy value of the investigated range. The recording of the PES was started when both the overall electrochemical current (as measured by the potential stat) and the photocurrent (as measured by the lock-in amplifier) were stabilized, which generally was achieved in the course of about 5 min. After each 2 nm wavelength change, the value of the photocurrent was measured after 30 s, a delay sufficient for the photocurrent to be stabilized. Additional experiments, where the photocurrent was measured twice successively at the same applied potential, showed that the photocurrent recorded in this way were stable within the duration of the experiments.

Raman Spectroscopy. The measurements presented here were conducted on a RM1000 Renishaw spectrometer equipped with an air-cooled CCD detector and a microscope. The excitation wavelength used was the 514 nm line of an Ar^+ ion laser. Spectra were acquired using a 50x (Na = 0.75) objective. Before each analysis, the output laser power was adjusted to avoid excessive heating of the samples. Using the acquisition conditions described above, the spectral resolution of the different systems was about 0.1 cm^{-1}, and the lateral resolution was about 1 μm. Typical acquisition times of individual spectra were in the 10−30 s range, depending on the signal/noise ratio needed. Raman images were obtained for each sample mounted on a XY table. During the scans, the full spectra were recorded and stored in a specific "image" file. Once the data had been collected, Raman images were created from the information in all the individual spectra. Data processing was mostly performed using the factory-supplied Renishaw WIRE 3.0 software. In particular, band-fitting procedures were used to extract the frequency and width of specific lines of interest.

Scanning Kelvin Probe Force Microscopy (SKPFM). The SKPFM instrument used for this investigation was the "Multimode V" from Bruker. Scanning of the surface was carried out in the interleave mode, in which the tip scans the topography first. This was followed by the surface potential scanning, in which the tip was raised by 100 nm and then kept at constant distance from the surface. A conductive tip with a typical tip radius of 10 nm and scan area of 1 μm × 1 μm was used. The surface potential of the specimen was mapped using SKPFM with and without UV light illumination. The UV light source was a DH-2000 lamp with the wavelength ranging from 200 to 1000 nm. The intensity of the lamp at 350 nm was approximately 110 μW/cm^2.

Optical Measurements. Optical diffuse reflectance measurements were carried out top provide information about the UV absorption characteristics of the TiO_2 coating, which in turn were used to determine the band gap of the semiconductor. A detailed description of the optical measurement setup is given elsewhere.[5]The diffuse reflectance of the UV−visible spectra (UV-2600 from SHIMADZY) was converted to the equivalent absorption using the Kubelka−Munk model.

RESULTS

Microstructural Characterization. *Crystallinity of the Coating.* The XRD measurements shown in Figure 1 illustrate that the coatings formed by the magnetron sputtering process consist mainly of TiO_2 in the anatase crystal structure. Additional peaks in the diffractogram originate from the substrate. However, the TiO_2 coating on Cu substrate shows additional peaks, which may correspond to Cu_2O, CuO, and TiO phases. The Scherer equation was used to acquire an estimate of the average crystallite size from the anatase 101

diffraction peak. The estimated size was found to be 22, 25, and 29 nm for the Cu, Ni, and Au substrates, respectively.

Surface Topography. The AFM pictures of the surface topography of TiO_2 on three different substrates are shown in Figure 2. The planar view of the TiO_2 surface shows that the coating on the Au and Ni substrates has a uniform columnar structure, while the coating on the Cu substrate shows large and small grains, which merge together at the surface.

Figure 3 shows high resolution scanning electron microscopy pictures of the surface of the various coatings. The appearance

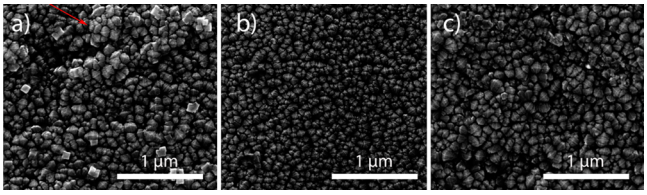

Figure 3. High-resolution scanning electron microscope pictures of TiO_2 coating on various substrates: (a) Cu, (b) Ni, and (c) Au.

of the coating is similar to that observed in AFM, with planar view of the columnar crystallites; however, the surface of the coating on the Cu surface shows cauliflower-type of growth in at some places (see red arrow), which can be partly influenced by the surface roughness of the copper.

Cross-Sectional TEM View of the Coating and Interface. Figure 4 shows the cross-sectional images of the coating and substrate-coating interface at low and high magnification. Thickness of the TiO_2 coating for the Ni and Au substrates was identified as approximately 850 nm. In contrast, the thickness of the TiO_2 coating on the Cu substrate (Figure 4a1, a2) is different because of the presence of an interface layer overlapping with the TiO_2. The TiO_2 layer was approximately 550 nm, whereas the layer showing a mixture of copper oxides and titanium oxides had a thickness of ~720 nm. The TiO_2 coating deposited on the Ni substrate is shown in Figure 4b1, b2. The Ni substrate is smooth and the coating is dense. A clear coating of the metal substrate interface can be observed. Similarly, the TiO_2 on Au presents a smooth interface without any intermediate oxide layer. The Au substrate has some nanoscale roughness, which is also observed during the coating growth.

Structural Properties. Figure 5 shows Raman spectra of the anatase coatings on Cu, Ni, and Au substrates. The spectra have

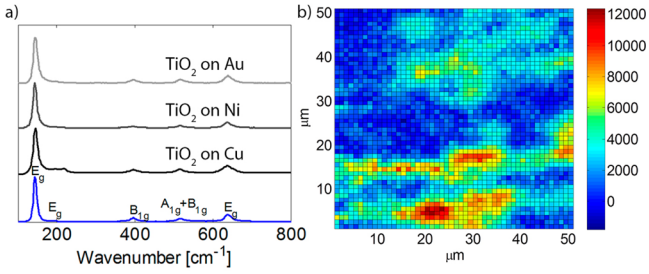

Figure 5. (a) Raman Spectra of the TiO_2 coatings on different substrates (*Y*-axis represents normalized intensity) and (b) mapping of intensity of Cu_2O oxide detected on the TiO_2 coating on Cu. (*Y*-axis scale bar is intensity [au]).

dominating peaks located at about 143, 197, 369, 516, and 638 cm^{-1}, which are the optical vibrational modes within anatase structure.

Anatase was detected on all mapped surfaces, whereas an additional Raman peak was detected at about 217.5 cm^{-1} for the TiO_2 coating on the Cu substrate (enlarged in the figure), which is attributed to Cu_2O. The Cu substrate has more roughness (seen in Figure 4a), which is reflected in the inhomogeneity of the coating. The mapping of the Cu_2O peak demonstrated an unequal distribution of the Cu oxide on the interface between the substrate and the coating (Figure 5b). The inhomogeneous signal of the Cu_2O seen in Figure 5b can be correlated with the top surface SEM imaging (Figure 3a) in which cauliflower-type of localized growths were observed.

The position of the most dominating peak was at ~143 cm^{-1} for the anatase TiO_2 powder. The peak positions of the TiO_2 samples can be seen in Figure 6 a1, b1, and c1. There are small peak shifts for the anatase coating on the nickel and gold substrates. These small shifts are characteristic of local small stress in the TiO_2 coating.

Figure 6a1, b1, and c1) shows a slight upshift in the dominating peak position of TiO_2 coatings on Au, which may be attributed to the stress in the coating. In contrast, for TiO_2 on Cu, a larger upshift is observed along with significant broadening of the line. As seen in Figure 6a1, a2, both maps are strongly correlated, i.e., the higher the upshift, the larger the line broadening. This is a strong indication of phonon

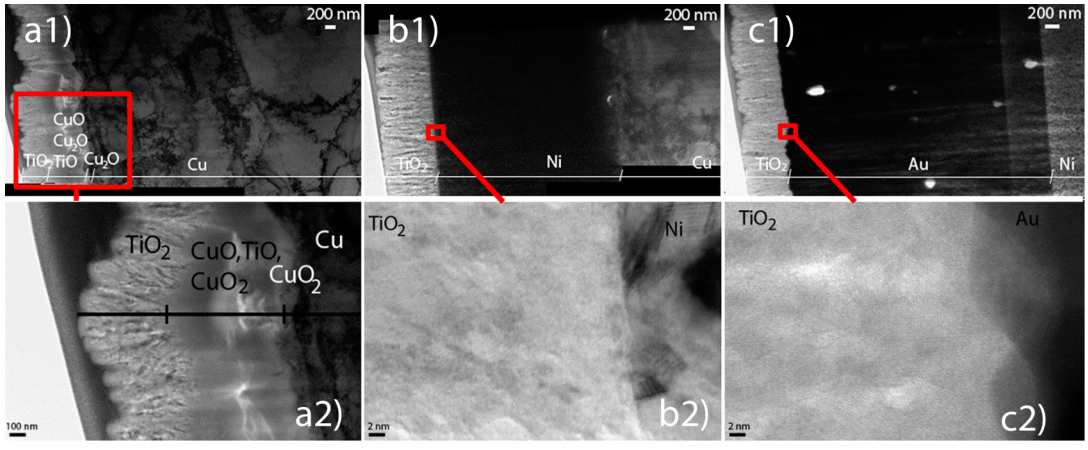

Figure 4. TEM cross-sectional images of the TiO_2 coating on: (a1, a2) Cu, (b1, b2) Ni, and (c1, c2) Au.

dx.doi.org/10.1021/am5059298 | ACS Appl. Mater. Interfaces 2014, 6, 22224−22234

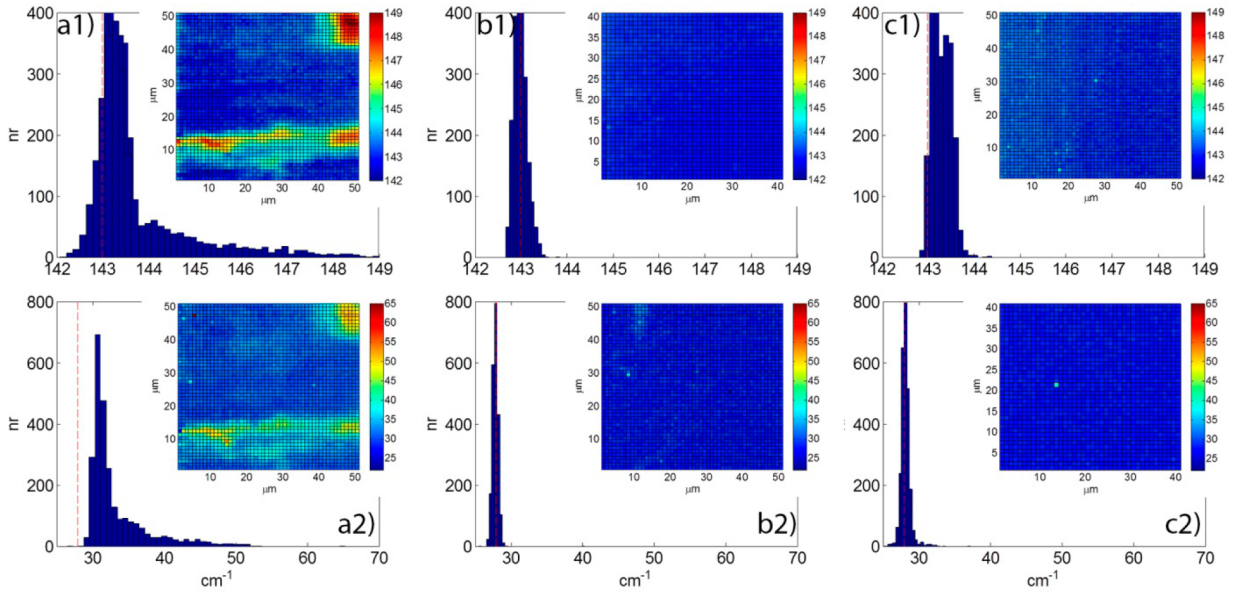

Figure 6. Histogram and reference line (red) together with a map of the surface for the peak postion of $E_g(\nu_6)$, on (a1) Cu, (b1) Ni, and (c1) Au, and for the peak broadening for $E_g(\nu_1)$ (a1) Cu, (b1) Ni, and (c1) Au.

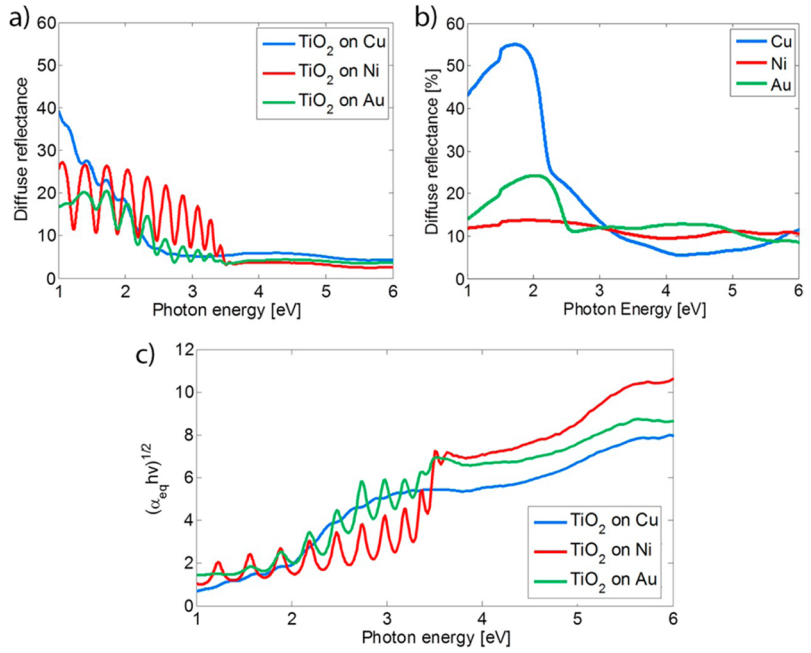

Figure 7. Diffuse reflectance spectra and calculated absorption coefficient as a function of photon energy: (a) TiO_2 coatings on various substrates, (b) spectra from bare substrates, and (c) square root of equivalent absorption from coatings on various substrates.

confinement phenomena, with the regions exhibiting larger broadening corresponding to the smallest grain sizes.

Photocatalytic Measurements. *Optical Spectrophotometry Studies.* Optical spectrophotometric measurements were carried out to measure the band gap of the TiO_2 coatings on various substrates, which is an indirect measure of the influence of the substrate material on the photocatalytic properties of the TiO_2 coating. The diffuse reflectance spectra of the substrate and the TiO_2 coating as a function of the wavelength of light are shown in Figure 7a, b. The diffuse reflectance for the TiO_2 coating was converted to the equivalent absorption coefficient using the Kubelka–Munk equation as shown in Figure 7c for various substrates.[5] The absorption coefficient data can be used to calculate the band gap, which enables a better comparison between the band gap values obtained from the optical and photo electrochemical studies. The interference fringes observed in Figure 7a, c are an indication of a transparent and homogeneous TiO_2 coating on Ni and Au.

The TiO_2 coating on Cu starts to absorb light in the visible domain starting at 2 eV and up to 3.40 eV. The absorption by the TiO_2 coating on Ni starts to increase at 3.28 eV and reaches a maximum at 3.50 eV. The absorption of TiO_2 on Au starts at 2.50 eV and reaches a maximum at 3.48 eV. The standard method for determining the band gap is to extrapolate the $(\alpha h\nu)^{1/2}$ to zero. The band gap values extracted using such extrapolation were 3.35 and 2.99 eV for Ni and Au, respectively.

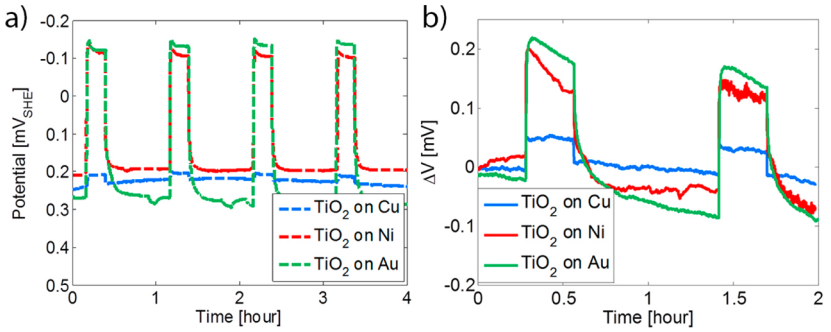

Figure 8. Photovoltage upon UV-activation of TiO_2 coatings on various substrates: (a) Open circuit potential measurements in aqueous medium and (b) SKPFM measurements in air.

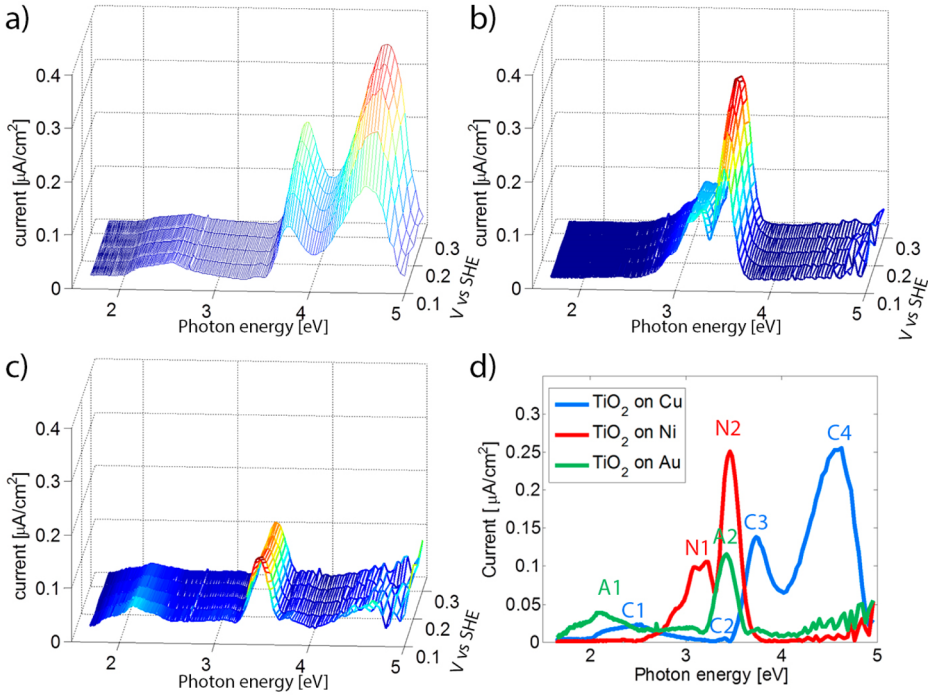

Figure 9. Photocurrent generated as a function of photon energy at various potentials for TiO_2 coating on: (a) Cu, (b) Ni, and (c) Au. (d) Comparison of all spectra at a potential of 0.14 V vs SHE.

Because of the shape of the absorption edge of TiO_2 on Cu, it was not possible to extract a band gap value. It is interesting to note that the absorption in the UV range is highest for TiO_2 on Ni.

The optical reflectance spectra of TiO_2 on Cu, Au, and Ni substrates are shown in Figure 7b. The spectra for Cu and Au shows typical features of the electron interband transition at a photon energy of 2 and 2.5 eV, respectively.[21,22]

Photovoltage Measurements. The photovoltage is an indirect indication of the energy of the photoexited electrons and therefore the location of the CB. The photo voltage was measured by two different methods, by monitoring the excitation voltage under open circuit conditions and by scanning kelvin probe force microscopy. Figure 8 summarizes the results from both experiments. As shown in Figure 5A, the open circuit potential of the samples under nonirradiation conditions is in the range of 0.35−0.2 V. The surface potential decreases (shown by the excitation peaks) significantly when the sample is irradiated with UV light. The excitation potential is around −0.12 V vs SHE (the potential change is approximately 0.39 and 0.25 V for Au and Ni, respectively) for the first excitation peak of TiO_2 on the Au and Ni substrates and 0.21 V vs SHE for TiO_2 on Cu; the potential change is around 0.03 V. The surface potential, upon UV-illumination, for TiO_2 on Au is slightly higher than that for TiO_2 on Ni, whereas the base potential of the TiO_2 sample on the Au substrate is slightly lower than that for TiO_2 on Ni. Au metal has a higher galvanic potential than Ni metal.

Photocurrent Measurements. PES was used in this work to acquire information on the origin of the photocurrents and the photon energy needed to perform the photocatalytic reaction. The resulting spectra are presented in Figure 9. Panels a, b, and c show the photocurrent recorded at several applied potentials for the TiO_2 coating on Cu, Ni, and Au substrate, respectively, whereas Figure 9d compares the photocurrent of the different samples at the same applied potential.

The results in Figure 9 clearly show that the photoelectrochemical behavior of our TiO_2 samples deposited on metallic substrates is different depending on the metal substrate: significant photocurrents are detected for photon energies well below the 3.2 eV band gap of anatase, namely in

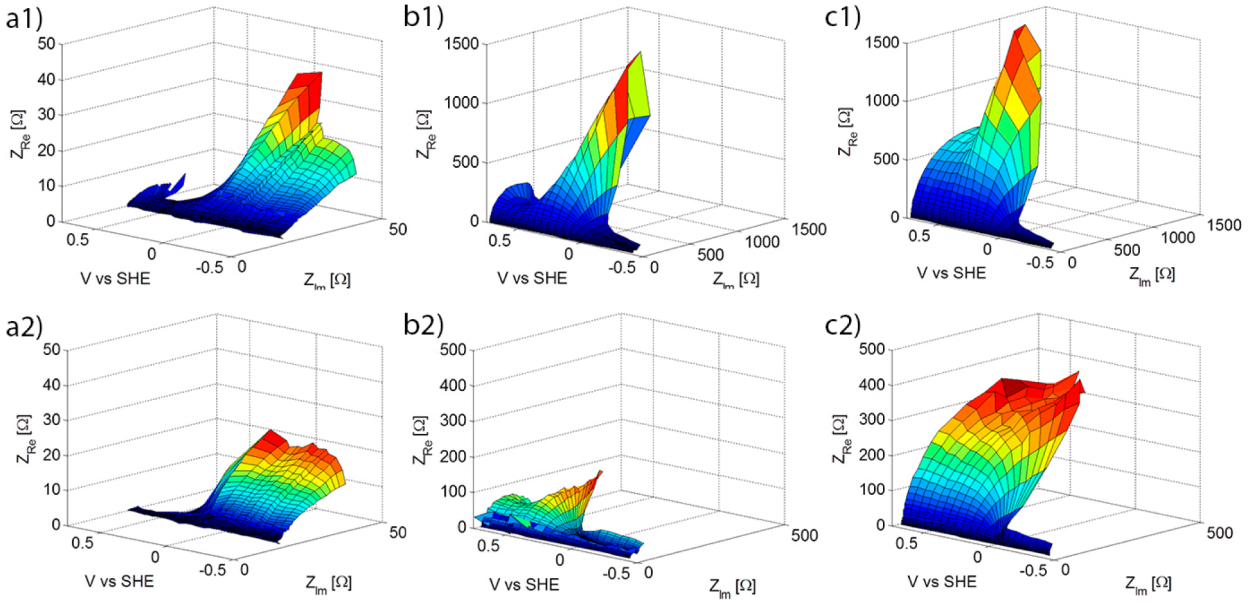

Figure 10. Nyquist plot mesured with and without UV light for TiO_2 coating on: (a1) Cu with out UV, (b1) nickel with out UV, (c1) Au with out UV, (a2) Cu with UV, (b2) nickel with UV, and (c2) Au with UV.

the range of 1.8 to 3.2 eV, and the photocurrent spectra exhibit several peaks, above as well as below the latter band gap.

It is also evident from Figure 9 that that the photocurrent, and therefore the photoelectrochemical behavior of the investigated samples, is strongly affected by the nature of the metallic substrate on which TiO_2 was deposited. For instance, it can be observed that the photocurrents globally increase by increasing the applied potential, and thus the band bending in TiO_2, for the TiO_2 coating on Ni and Cu substrate (Figure 9a, b). This is in contrast with the TiO_2 coating Au substrate. Furthermore, the photocurrent peaks at photon energies below the band gap of anatase (the shoulder on N1, C1, A1) are located at different energies. However, it is noteworthy that whatever the sample, normalizing the PES spectra at the photocurrent maximum, the peak corresponding to the energy of the band gap of anatase, shows that the shape of the photocurrent spectrum of a given sample is nearly independent of the potential.

As indicated above, the photocurrent energy spectra in Figure 9d were measured for all the samples at the same applied potential, 0.14 V vs SHE, which is the lowest tested potential in this work. The onset of the main photocurrent (the one due to electron/hole generation and separation in the TiO_2 coatings) is observed at 3.50, 3.28, and 3.21 eV, and it reaches a maximum at 3.73 eV (marked with C3), 3.46 eV (marked with N2), and 3.43 eV (marked with A2) for TiO_2 on Cu, Ni, and Au, respectively. These results are in agreement with the values of the maximum absorption edge obtained from the diffuse reflectance measurements (3.73, 3.50, and 3.48 eV for TiO_2 on Cu, Ni, and Au respectively).

Regarding the additional contributions to the photocurrent, it is proposed that the photocurrent peak (A1) at 2.3 eV observed for TiO_2 on Au could be due to the interband transitions of the free electrons from Au. The amplitude of the peak N1, observed in the photocurrent spectrum of TiO_2 on Ni and overlapping the one of the photocurrent from TiO_2 (N2), seems to be potential independent in the investigated potential range. This suggests that the quantum yield of this photocurrent contribution is controlled by other phenomena than the electron−hole pairs separation formed in the anatase coating. For the Cu samples, four peaks are exhibited in the photocurrent spectra, including one in the visible region (C1), which indicates absorption corresponding to the band gap of the CuO_2 formed on the substrate or interband transition in copper (the peak is visible in the diffuse reflectance spectra on the substrate, Figure 7b). The small photocurrent peak around the bandgap of anatase (C2), starting near 3.2 eV, could originate from zones on the coating on Cu where the TiO_2 grains are sufficiently large. However, the onset of the highest contribution to the photocurrent is around 3.50 eV and reaches a maximum value at 3.7 eV, indicating higher band gap of the TiO_2 coating on Cu; this is, expected based on the quantum confinement in TiO_2 detected for this sample using Raman spectroscopy. Finally, the high photocurrent peak at around 4.5 eV (C4) could indicate metal interband transitions in the substrate; the same effect can be seen in the diffuse reflectance spectra of the substrate (Figure 7b), where there is a trough (absorption peak) around 4.5 eV.

The photocurrent vs energy curve for TiO_2 on Ni shows a peak (N1) overlapping the photocurrent formed from TiO_2 (N2). The peak (N1) does not increase or decrease with increased potential, indicating that the efficiency of the interface excitation is at its maximum.

The photocurrent curve for TiO_2 on Cu shows four peaks including one in the visible region (C1) indicating absorption corresponding to the band gap of the CuO_2 and TiO. There is a small photocurrent peak around the band gap of anatase (C2), or starting at 3.19 eV, which originates from places of the coating on Cu where there is no quantum confinement. However, the highest photocurrent peak starts at 3.50 eV and reaches a maximum at 3.7 eV, indicating a higher band gap of the TiO_2 coating on Cu. The quantum confinement, as detected with the use of Raman spectroscopy, is known to slightly increase the band gap of the coating. The high current peak at around 4.5 eV (C4) is indicative of metal interband transitions in the substrate; the same effect can be seen in the diffuse reflection spectra of the substrate (Figure 7b) where there is a reflectance trough (absorption peak) around 4.5 eV

Photo Electron Impedance Spectroscopy. EIS measurements were used to understand the resistance of the chemical reaction, involving the TiO_2 coating on different substrates. Figure 10 shows the Nyquist plot of TiO_2 coatings measured without UV light (Figure 10a1, b1, and c1) and with UV-light (Figure 10a2, b2, and c2). The EIS graphs consist of semicircles and the diameter of the semicircle indicates how the reaction resistance varies depending on the substrate.

For all substrates with TiO_2 coating illuminated by UV-light, the diameter of the semicircles decreased indicating a reduction in the reaction resistance (the scales of the *Y*-axis for Au and Ni is different from that for Cu). The TiO_2 on Cu showed significantly lower reaction resistance both with and without UV light. Also the shape of the Nyquist plot for TiO_2 on Cu is different than that of the other substrates.

Furthermore, the reaction resistance was found to be highest close to the open circuit potential, while the reaction resistance decreased for TiO_2 on Cu and Ni for a potential more positive than the open circuit potential. The TiO_2 on Au with UV-light had approximately the same reaction resistance at potential values close to the open circuit potential and more positive potentials. The same behavior was seen in the photocurrent measurements, namely increased current was observed for TiO_2 on Ni and Cu at higher potentials, whereas the TiO_2 on Au did not show any effect.

DISCUSSION

Structure of TiO_2 Coating on Various Substrates. The XRD measurements confirmed that the coating consists of anatase structure on all substrates without any significant contribution from rutile. The surface view SEM and AFM images showed that the coating was characterized by columnar growth with pyramidal cap shape. However, the TiO_2 coating on Ni and Au showed a homogeneous structure, while the coating on Cu was inhomogeneous with wavy structure consisting of regions with cauliflower-type of growth. The cross-sectional TEM images also showed differences in coating morphologies from the interface to the top on the various substrates. The reaction between O and Ti during the deposition process leads to the formation of TiO_2, whereas the O reaction with substrate may lead to the formation of a thin layer of metal substrate oxide. The stability of the substrate metal oxides compared to the formation of TiO_2 is based on the Gibbs free energy for oxide formation as can be seen in Figure 11 for the temperature range of interest. The rate of growth also depends on the time of interaction, which is expected to depend on the TiO_2 coating growth rate.

Figure 11 shows that for all the metal substrates, free energy of oxide formation is higher than that of TiO_2, therefore, preferential TiO_2 formation dominates. This is in agreement with the TEM observation of a cross-section for TiO_2 grown on Ni and Au for which no oxide layer was found. The interface of TiO_2 on the Ni and Au substrates showed a diffusion interface with a gradual change in composition across the TiO_2 film (2 nm for Ni and around 4 nm for Au), but no compound formation on the interface.[24] The roughness of the Au substrate affects the columnar growth. Raman measurements showed slight peaks upshift indicating small compressive stress in the TiO_2 coating on Au substrate.

Coating on the Cu substrate on the other hand showed an interfacial oxide layer formation, although the Gibbs free energy for formation of copper oxides is higher than that for TiO_2. In this case two layers between the metal substrate and the coating

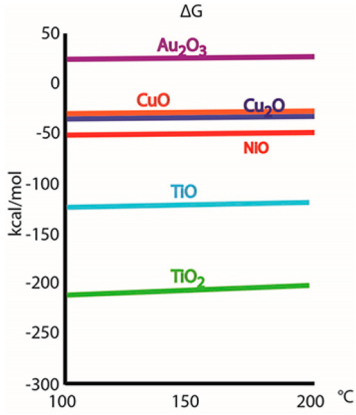

Figure 11. Schematic of a simple Ellingham diagram for oxides of Ti, Ni, Cu, and Au[23]

were detected under TEM, namely, CuO_2 on the substrate and a mixture of TiO and copper oxide (720 nm thick) sandwiched between the Cu oxide and the TiO_2 coating. Copper oxide could be a mixture of CuO and Cu_2O based on the XRD result; however the Raman spectra showed only evidence for Cu_2O formation. Although two layers were distinguishable in the TEM, it was difficult to determine the composition of each layer. The Raman spectra showed an upshift and broadening of the E_g peaks of anatase indicating phonon confinement, which occurred as a result of small size and the geometrical effect of the grains.[25,26] The peak shift in general can be attributed to the stress in the coating, nonstoichiometry, and phonon confinement.[27]The small grain size in the coating results in a larger band gap. The formation of the interfacial layer might be explained by a mixture of the compound interface and recrystallization of the copper substrate surface. The compound interface is most common in oxygen active metal coatings on a metallic oxide substrate.[24] The compound interface occurs when the deposited atoms are condensed to the substrate, causing an exothermic reaction. The heat energy released into the Cu substrate is used for forming higher energy oxides than TiO_2, for example TiO and CuO at the interface. Because of the low recrystallization temperature of Cu (about 120 °C, which is just below the deposition temperature of 150 °C), Cu recrystallization may enlarge the interfacial zone by forming new grains from older Cu grains. The new grains may form increased interfacial area that can promote the formation of copper oxides.

The mixed oxide interface found between the copper substrate and TiO_2 coating blocks contact between the two. Giolli et al. showed that the TiO_2 coating synthesis with electric arc PVD resulted in islands of TiO_2 clusters rather than continuous coating in the substrate-coating interface. The explanation given for this effect is that Cu atoms can migrate along the grain boundaries of the TiO_2 coating. The interaction of the Cu atoms and TiO_2 coating could be prevented by reducing synthesis pressure and decreasing the temperature.[28]

Photocatalytic Activity of TiO_2. Results from photon absorption (Figure 7), photocurrent (Figure 9), and EIS (Figure 10) measurements reveal that the photocatalytic activity of the TiO_2 coating varies depending on the nature of the metal substrate. This is consistent with the interface structure observed in the TEM (Figure 4) and the Raman spectroscopy results (Figure 5). There is some correlation between the results from absorption spectra measured by

diffused reflectance (Figure 7) and the photocurrent (Figure 9) measurements where the maximum photocurrent occurred at photon energy of 0.07, 0.04, and 0.05 eV prior to the maximum energy absorptions edge for Cu, Ni and Au respectively (Table 1). However, the deduced band gap values from the spectra did

Table 1. Estimated Band Gap and Photon Energy for Maximum Current/Absorption of TiO_2 from Optical and Photoelectrochemical Testing[29]

	TiO_2 on Cu		TiO_2 on Ni		TiO_2 on Au	
	OPS	PEC	OPS	PEC	OPS	PEC
photon energy for max absorption & current (eV)	3.80	3.73	3.50	3.46	3.48	3.43
band gap (eV)		3.50	3.35	3.28	2.99	3.21

not provide a good correlation between the techniques. The photocurrent energy spectrum showed a clear peak at the initiation of the formed photocurrent, due to excitation of the electrons to the CB. However, the absorption measured by diffuse reflectance did not show a clearly distinguishable sharp absorption peak.

The absorption and photocurrent energy spectra for TiO_2 coatings on various substrates are in agreement with the interface morphology observed by TEM and the Raman spectroscopy measurements. Similarly, the EIS results showed varied behavior in a Nyquist plots depending on the substrate. The reaction resistance of the TiO_2 coating on Ni had the largest change when measured in the dark and under UV-illumination, indicating the highest photocatalytic activity. Moreover, the TiO_2 coating on nickel showed the largest photocurrent peak (Figure 9), and the highest absorption value measured by diffuse reflectance, supporting the EIS result of the highest photocatalytic activity of TiO_2 on Ni. Studies related to Ni as a doping agent have reported an increase in the photocatalytic activity of TiO_2 in the UV range and a shift in the absorption to the visible range. The reason for better photocatalytic activity with Ni doping is not yet fully understood, but the bridging of energy bands of Ni to the VB of TiO_2, thus reducing the band gap locally, has been proposed.[15,30−32] A simple energy diagram of TiO_2 is presented in Figure 12, together with the band structure of Cu (II) oxide, Ni, and Au. The difference between the energy states of CB and VB is 3.2 eV for anatase TiO_2. The measured energy state can be converted to standard hydrogen electrode (SHE) for a given pH condition. The potential of the VB and CB of TiO_2 in an electrolyte of pH 5.5 (the pH of electrolyte used for the experiments) are 2.8 V and −0.45 V, respectively. The band structure shown in Figure 12 can be used to explain how the metals influence the photocatalytic activity of TiO_2. The measurements of TiO_2 on Ni showed two overlapping photocurrent peaks at photon energy of 3.20 and 3.46 eV. The same overlapping bands can be seen in the absorption spectra at photon energy of 3.5 and 3.6 eV. The two overlapping peaks might be caused by the interaction of Ni with the VB of TiO_2. This will rise the position of VB in TiO_2, while lowering the corresponding CB formed at the interface between the TiO_2 coating and Ni. As a result, the band gap at the interface between the coating and the substrates is reduced.

In the photocurrent energy spectra for TiO_2 on Ni and Cu, more photocurrent was generated as the applied positive potential was closer to the VB of TiO_2 or the potential of the

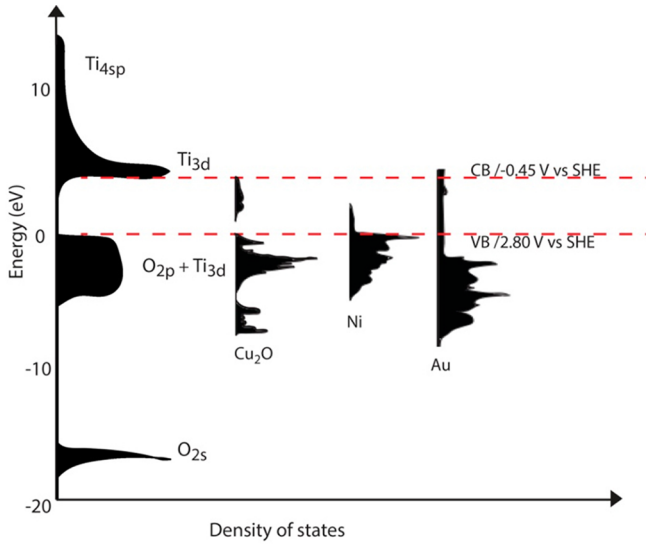

Figure 12. Simplified band energy diagram of TiO_2 in anatase form,[33] Au,[34] Ni,[34] and Cu(II)oxide.[35]

two metals. The same behavior was not observed for TiO_2 on Au. Furthermore, the spectra showed a current in the visible range for TiO_2 on Au. The measurements indicate that the TiO_2 on Au can easily transfer electrons to the CB of TiO_2. The energy band for Au in Figure 12 shows an overlap with the CB for TiO_2, therefore facile electron transfer is possible.

In the high photon energy regime (above 4 eV) the substrate might have significant influences; Figure 7b shows low diffuse reflectance, equivalent to high absorption, for the substrate materials. The high photon energy taken up by the substrate for nickel substrate might stimulate the electron in the metal. However, because of the band structure of the metal and the depth of activation, the stimulated electrons might decay to original sate before reaching the surfaces and produce photocurrent, with re-emissions of the photon energy in the form of heat. Negligible photocurrent was detected for energy higher than 4 eV for TiO_2 on Ni. The TiO_2 on Cu produce a photocurrent peak around 4.5 eV, the same feature is visible in the reflection spectra of the substrate; where there is a valley visible slightly before 4.5 eV, or with lowest peak of 4.25 eV. Due to the band structure of Cu and CuO_2, the electron transitions occurring might be transferred to the surfaces in the form of the photocurrent. Moreover it is important to note that the Kubelka−Munk method is not well understood in the high energy regime. The reaction resistance of TiO2 on Cu measured with photoimpedance. The reaction resistance of TiO_2 on Cu measured with photoimpedance is low both in the dark and under UV-illumination. Furthermore, the excitation potential from OCP and SKPFM measurements for TiO_2 on Cu was significantly lower than for TiO_2 on the other metal substrate. The OCP, SKPFM, and photon impedance measurements indicated low energy photon excitation. The Raman spectroscopy detected Cu_2O and phonon confinement in the TiO_2 coating. The band gap of Cu_2O is on average 2.1 eV and the maximum current generated at the quantum confinement for the TiO_2 coating was found to be 3.7 eV. The amplitude of the photo potential depends mainly on the electron-hole pair's generation yield, and on their recombination rates. Among the recombination paths is the redox reaction; where a photo-electron and a photo-hole are simultaneously transferred to two different redox species in the electrolyte (both cathodic and

anodic reactions, as in corrosion). Moreover, it has been reported that photon transitions within Cu_2O can reduce Cu_2O to metallic Cu.[36] The redox reaction may strongly reduce the photo potential. Furthermore the UV-lamp used for the EIS and the OCP had maximum intensity at 350 nm (3.54 eV) hence not reaching the energy of the band gap of the quantum confinement for the TiO_2 coating on the Cu substrate. The UV-lamp used for the EIS and the OCP was had maximum intensity at 350 nm hence not reaching the energy of the band gap of the quantum confinement for the TiO_2 coating on the Cu substrate. The measured OCP and photoimpedance indicated that the excitation voltage of TiO_2 on Cu is due to exited electrons in the CB of Cu_2O. The electron photon transition within Cu_2O can be reduced Cu_2O to metallic Cu, which might have influenced the photocurrent measured.[36]

CONCLUSION

- The XRD measurements demonstrated that the magnetron sputtered TiO_2 coating possessed anatase structure on all substrates, and the SEM and AFM images showed a columnar growth with pyramidal shape. The surface of the TiO_2 coating on copper substrate was inhomogeneous with a cauliflower-type of growth in a number of places.
- The TEM cross-sectional images showed a relatively sharp interface layer for TiO_2 on Ni and Au, while the TiO_2 coating on copper showed a two-layered structure with a layer of CuO and a mixture of Cu_2O and TiO_2.
- Results from the Raman spectroscopy measurements revealed possible quantum confinement in the TiO_2 coating on copper limiting its photocatalytic behavior. However, the results showed only the presence of Cu_2O.
- The OCP and Kelvin probe measurements gave light excitation voltage of TiO_2 on Au and Ni of −0.12 V from the base potential of 0.25 and 0.19 V for Ni and Au, respectively. However, TiO_2 on Cu has an light excitation potential of 0.13 V from the base potential of 0.22 V.
- The diffuse reflectance measurements showed high absorption for Cu in the visible region starting at 2.0 eV. The maximum absorption edge of the photocatalytic TiO_2 from optical measurements was found to be 3.73, 3.50, and 3.48 eV for TiO_2 on Cu, Ni, and Au, respectively.
- The photocurrent energy spectra showed that the maximum of the photocurrent peak from the TiO_2 coating corresponds to photon energy levels of 3.73, 3.46, and 3.43 eV for TiO_2 on Cu, Ni and Au, respectively. Photocurrent peaks for Ni showed overlapping peaks, indicating bridging between Ni and the TiO_2 band. The TiO_2 coating on Ni showed the highest photocurrent peak.
- The electrochemical impedance measurements showed decrease in the reaction resistance upon UV-illumination for Ni and Au, whereas similar behavior was not observed for TiO_2 on copper.

AUTHOR INFORMATION

Corresponding Author

*E-mail: sdav@mek.dtu.dk.

Notes

The authors declare no competing financial interest.

ACKNOWLEDGMENTS

The authors acknowledge funding from the Danish Advanced Technology Foundation AMAS project and SETNanoMetro, EU Project. R.S. thanks BQR-3b 2014-Univ Lille1 for the financial support for this collaboration. The authors also thank Perter Westerman and Io Mizushima for help related to the preparation of Au and Ni substrates.

REFERENCES

(1) Zhao, J.; Yang, X. Photocatalytic Oxidation for Indoor Air Purification: a Literature Review. *Build Environ.* **2003**, *38*, 645−654.
(2) Chong, M. N.; Jin, B.; Chow, C. W. K.; Saint, C. Recent Developments in Photocatalytic Water Treatment Technology: a Review. *Water Res.* **2010**, *44*, 2997−3027.
(3) Augugliaro, V.; Loddo, V.; Pagliaro, M.; Palmisano, G.; Palmisano, L.; *Clean by Light Irradiation: Practical Applications of Supported TiO_2*; RSC Publishing: Cambridge, U.K.. 2010, 2−5.
(4) Diebold, U. The Surface Science of Titanium Dioxide. *Surf. Sci. Rep.* **2003**, *48*, 53−229.
(5) Daviðsdóttir, S.; Canulescu, S.; Dirscherl, K.; Schou, J.; Ambat, R. Investigation of Photocatalytic Activity of Titanium Dioxide Deposited on Metallic Substrates by DC magnetron sputtering. *Surf. Coat. Technol.* **2013**, *216*, 35−45.
(6) Jia-long, Y.; Ying, L.; Fu, W. New Application of Stainless Steel. *Appl. Catal.* **2006**, *3*, 62−66.
(7) Hirakawa, Y.; Jimbo, R.; Shibata, Y.; Watanabe, I.; Wennerberg, A.; Sawase, T. Accelerated Bone Formation on Photo-Induced Hydrophilic Titanium Implants: an Experimental Study in the Dog Mandible. *Clin Oral Implants Res.* **2013**, *24* (Suppl A), 139−44.
(8) Jimbo, R.; Ono, D.; Hirakawa, Y.; Odatsu, T.; Tanaka, T.; Sawase, T. Accelerated Photo-Induced Hydrophilicity Promotes Osseointegration: an Animal Study. *Clin Implant Dent Relat Res.* **2011**, *13*, 79−85.
(9) Unosson, E.; Welch, K.; Persson, C.; Engqvist, H. Stability and Prospect of UV/H_2O_2 Activated Titania Films for Biomedical use. *Appl. Surf. Sci.* **2013**, *285*, 317−323.
(10) Kwon, D.-H.; Kim, K. M.; Jang, J. H.; Jeon, J. M.; Lee, M. H.; Kim, G. H.; Li, X.-S.; Park, G.-S.; Lee, B.; Han, S.; Kim, M.; Hwang, C. S. Atomic Structure of Conducting Nanofilaments in TiO_2 Resistive Switching Memory. *Nat. Nanotechnol.* **2010**, *5*, 148−53.
(11) Kimiagar, S.; Nahal, A.; Mohammadizadeh, M. R.; Elahi, T. G. Influence of Substrate on the Hydrophilicity and Photocatalytic Properties of TiO_2 Nano-Layers. *Phys. Scr.* **2013**, *88*, 025604.
(12) Paola, A. D.; Ikeda, S.; Marcì, G.; Ohtani, B.; Palmisano, L. Transition Metal Doped TiO_2: Physical Properties and Photocatalytic Behaviour. *Int. J. Photoenergy.* **2001**, *3*, 171−176.
(13) Sunada, K.; Watanabe, T.; Hashimoto, K. Bactericidal Activity of Copper-Deposited TiO_2 Thin Film under Weak UV Light Illumination. *Environ. Sci. Technol.* **2003**, *37*, 4785−47859.
(14) Carneiro, J. T.; Yang, C.-C.; Moma, J. A.; Moulijn, J. A.; Mul, G. How Gold Deposition Affects Anatase Performance in the Photocatalytic Oxidation of Cyclohexane. *Catal. Lett.* **2009**, *129*, 12−19.
(15) Iwaszuk, A.; Nolan, M.; Jin, Q.; Fujishima, M.; Tada, H. Origin of the Visible-Light Response of Nickel (II) Oxide Cluster Surface Modi fied Titanium (IV) Dioxide. *J. Phys. Chem. C* **2013**, *117*, 2709−2718.
(16) Spagnol, V.; Cachet, H.; Baroux, B.; Sutter, E. Influence of Sub-Band-Gap States on Light Induced Long-Lasting Super-Hydrophilic Behavior of TiO_2. *J. Phys. Chem. C* **2009**, 3793−3799.
(17) Miyauchi, M.; Nakajima, A.; Watanabe, T.; Hashimoto, K. Photocatalysis and Photoinduced Hydrophilicity of Various Metal Oxide Thin Films. *Chem. Mater.* **2002**, *14*, 2812−2816.
(18) Haque, S. A.; Tachibana, Y.; Willis, R. L.; Moser, J. E.; Gra1tzel, M.; Klug, D. R.; Durrant, J. R. Parameters Influencing Charge Recombination Kinetics in Dye-Sensitized Nanocrystalline Titanium Dioxide Films. *J. Phys. Chem. C* **2000**, *104*, 538−547.
(19) Kikuyama, H.; Waki, M.; Miyashita, M.; Yabune, T.; Mai, C. C.; Looney, J. C. Thermally Stimulated Deep-Level Impedance Spectroscopy. *J. Electrochem. Soc.* **1996**, *143*, 4066−4074.

(20) Daviðsdóttir, S.; Dirscherl, K.; Shabadi, R.; Canulescu, S.; Ambat, R. Nanoscale Surface Potential Imaging of the Photocatalytic TiO_2 Films on Aluminum. *RSC Adv.* **2013**, *3*, 23296−23302.
(21) Roberts, S. Optical Properties of Copper. *Phys. Rev.* **1960**, *118*, 1509−1518.
(22) Loebich, O. The Optical Properties of Gold. *Gold Bull.* **1972**, *5*, 2−10.
(23) HSC Chemistry, Software for Process simulation, Reactions Equations, Heat and Material Balances, Heat Loss Calculator, Equilibrium Calculations, Electrochemical Cell Equilibriums, Eh-pH Diagrams − Pourbaix diagram, Tpp Diagrams − Stability diagrams, Miner. Available at: http://www.hsc-chemistry.net/ (accessed May 16, 2014).
(24) Mattox, D. M. *Handbook of Physical Vapor Deposition (PVD) Processing*, second ed.; Elsevier: Amsterdam, 2010; pp 333−398.
(25) Chen, X.; Mao, S. S. Titanium Dioxide Nanomaterials: Synthesis, Properties, Modifications, and Applications. *Chem. Rev.* **2007**, *107*, 2891−2959.
(26) Yu, H.; Li, J.; Loomis, R. A.; Wang, L.-W.; Buhro, W. E. Two- versus Three-Dimensional Quantum Confinement in Indium Phosphide Wires and Dots. *Nat. Mater.* **2003**, *2*, 517−20.
(27) Georgescu, D.; Baia, L.; Ersen, O.; Baia, M.; Simon, S. Experimental Assessment of the Phonon Confinement in TiO_2 Anatase Nanocrystallites by Raman Spectroscopy. *J. Raman Spectrosc.* **2012**, *43*, 876−883.
(28) Giolli, C.; Borgioli, F.; Fabio, A. D.; Credi, A.; Fabio, A. D.; Fossati, A.; Muniz, M. M.; Parmeggiani, S.; Rizzi, G.; Scrivani, A.; Troglio, S.; Tolstoguzov, A.; Zoppi, A.; Bardi, U. Characterization of TiO2 Coatings Prepared by a Modified Electric Arc-Physical Vapour Deposition System. *Surf. Coat. Technol.* **2007**, 13−22.
(29) The estimated band gap and photon energy corresponds to peak value of absorption/current from optical absorption (OPS) (Figure 7) and photocurrent measured as a function of photon energy (PES) (wavelength of incident light, Figure 9).
(30) Bhosale, R. R.; Pujari, S. R.; Lande, M. K.; Arbad, B. R.; Pawar, S. B.; Gambhire, A. B. Photocatalytic Activity and Characterization of Sol−Gel-Derived Ni-Doped TiO_2-Coated Active Carbon Composites. *Appl. Surf. Sci.* **2012**, *261*, 835−841.
(31) Kim, H. D.; Lee, S. K.; Kim, Y.-S.; Chung, Y.-C.; Kim, S.-J. Photocatalytic Activity of Ni 8 wt%-Doped TiO_2 Photocatalyst Synthesized by Mechanical Alloying Under Visible Light. *J. Am. Ceram. Soc.* **2006**, *89*, 515−518.
(32) Niishiro, R.; Kato, H.; Kudo, A. Nickel and Either Tantalum or Niobium-Codoped TiO_2 and $SrTiO_3$ Photocatalysts with Visible-Light Response for H_2 or O_2 Evolution from Aqueous Solutions. *Phys. Chem. Chem. Phys.* **2005**, *7*, 2241−2245.
(33) Scanlon, D. O.; Dunnill, C. W.; Buckeridge, J.; Shevlin, S. A.; Logsdail, A. J.; Woodley, S. M.; Catlow, C. R. A.; Powell, M. J.; Palgrave, R. G.; Parkin, I. P.; Watson, G. W.; Keal, T. W.; Sherwood, P.; Walsh, A.; Sokol, A. A. Band Alignment of Rutile and Anatase TiO_2. *Nat. Mater.* **2013**, *12*, 798−801.
(34) McPherson, D. J.; Supansomboon, S.; Zwan, B.; Keast, V. J.; Cortie, D. L.; Gentle, A.; Dowd, A.; Cortie, M. B. Strategies to Control the Spectral Properties of Au−Ni Thin Films. *Thin Solid Films.* **2014**, *551*, 200−204.
(35) Chen, X.; Parker, D.; Du, M.-H.; Singh, D. J. Potential Thermoelectric Performance of Hole-Doped Cu_2O. *New J. Phys.* **2013**, *5*, 043029.
(36) Hara, M.; Kondo, T.; Komoda, M.; Ikeda, S.; Shinohara, K.; Tanaka, A. Cu_2O as a Photocatalyst for overall Water Splitting under Visible Light Irradiation. *Chem. Commun.* **1998**, *2*, 357−358.